Observation of sea salt fraction in sub-100 nm diameter particles at Cape Grim

Luke T. Cravigan[1], Zoran Ristovski[1], Robin L. Modini[2], Melita D. Keywood[3], John L. Gras[3].

1. International Laboratory for Air Quality and Health, Queensland University of Technology, Brisbane, Australia.
2. Ecole Polytechnique Federale de Lausanne, Lausanne, Switzerland.
3. CSIRO Ocean and Atmosphere Flagship, Aspendale, Australia.

Corresponding author: Zoran Ristovski
International Laboratory for Air Quality and Health (ILAQH)
Queensland University of Technology (QUT)
Brisbane, QLD 4000, Australia.
PH: +61 731381129.
E-mail: z.ristovski@qut.edu.au

Abstract

Volatility-hygroscopicity tandem differential mobility analyser (VH-TDMA) measurements were used to infer the composition of sub-100 nm diameter Southern Ocean marine aerosols at Cape Grim in November and December 2007. This study focuses on a short lived high sea spray aerosol (SSA) event on 7-8 December with two externally mixed modes in the Hygroscopic Growth Factor (HGF) distributions (90% RH), one at HGF > 2 and another at HGF ~1.5. The particles with HGF > 2 displayed a deliquescent transition at 73-75% RH, and were non-volatile up to 280°C, which identified them as SSA particles with a large inorganic sea salt fraction. SSA HGFs were 3 – 13% below those for pure sea salt particles, indicating an organic volume fraction (OVF) of up to 11 – 46%. Observed high inorganic fractions in sub-100 nm SSA is contrary to similar, earlier studies. HGFs increased with decreasing particle diameter over the range 16 – 97 nm, suggesting a decreased OVF, again contrary to earlier studies. SSA comprised up to 69% of the sub-100 nm particle number, corresponding to concentrations of 110-290 cm^{-3}. Air mass back trajectories indicate that SSA particles were produced 1500 km, 20-40 hours upwind of Cape Grim. Transmission electron microscopy (TEM) and X-ray spectrometry measurements of sub-100 nm aerosols collected from the same location, and at the same time, displayed a distinct lack of sea salt. Results herein highlight the potential for biases in TEM analysis of the chemical composition of marine aerosols.

Key points:

- Characterisation of high concentration sea spray aerosol (SSA) event.
- Sub-100 nm SSA organic volume fraction of up to 11 – 46% and size independent.
- Free tropospheric entrainment coincided with enhanced SSA concentrations.

Keywords:

marine aerosol, sea spray, CCN, hygroscopic growth, deliquescence, Cape Grim, entrainment.

Index terms:

Aerosols and particles (0305), Air/sea constituent fluxes (0312), Constituent sources and sinks (0322), Troposphere: constituent transport and chemistry (0368), Clouds and aerosols (3311).

1. Introduction

The remote marine aerosol, free from direct continental influences, plays an important role in the global climate by directly scattering incoming solar radiation and acting as cloud condensation nuclei (CCN) [*Andreae and Rosenfeld*, 2008]. Recent modelling has highlighted the need for a greater understanding of aerosol forcing in pristine environments, indicating that natural emissions make up 45% of the variance in aerosol forcing since 1750 [*Carslaw et al.*, 2013]. Sea spray aerosols (SSA) are an important marine aerosol class. They are primary particles produced from the bursting of bubbles at the oceans surface or from wind shear. Observations at or near cloud level have indicated that SSA can contribute significantly to the marine CCN. For example, SSA formed 20% of the total potential CCN at supersaturations between 0.2 and 0.43 during a recent study in the mid-latitudinal Pacific Ocean [*Blot et al.*, 2013]. Despite the climatic importance of primary marine aerosols there are significant uncertainties regarding the production mechanisms and chemical composition of the sub-100nm diameter SSA. In particular, the factors that control SSA concentrations in the atmosphere and the organic enrichment of sub-100nm diameter primary marine aerosols relative to water biology are poorly understood [*Gantt and Meskhidze*, 2013].

Recent studies have simulated the production of SSA in-situ and under controlled laboratory conditions by bubbling air through seawater [*Modini et al.*, 2010], by continuously plunging water [*Fuentes et al.*, 2010], and/or through wave action [*Prather et al.*, 2013]. These methods have consistently detected a dominant mode in the SSA number distribution at sizes less than 100 nm dry diameter [*Fuentes et al.*, 2010; *Modini et al.*, 2010; *Bates et al.*, 2012] with the exception of the wave chamber method, where a dominant mode centred at 160 nm was observed [*Prather et al.*, 2013]. All of the systems produce particles down to 10 nm in diameter. When scaled to real oceanic conditions, the bubble chamber data generally suggest SSA should consistently form the largest fraction of the total marine aerosol in remote

environments [*de Leeuw et al.*, 2011]. In addition, a recent parameterisation has suggested the presence of an SSA flux mode at approximately 20 nm [*Ovadnevaite et al.,* 2014]. Despite this, observations of sub-100 nm diameter SSA particles in the marine boundary layer (MBL) are relatively scarce, even under high wind conditions. It is not understood why this is the case [*Berg et al.*, 1998; *Kreidenweis et al.*, 1998; *Zhou et al.*, 2001; *Lewis and Schwartz*, 2004; *Swietlicki et al.*, 2008], although loss processes such as wet deposition likely play an important role [*Blot et al.*, 2013].

Tandem Differential Mobility Analyser (TDMA) data illustrate the scarcity of SSA observations well. TDMA techniques are well suited to the study of remote marine aerosols since they are able to differentiate the main marine aerosol types i.e. SSA, non-sea salt sulfates (nss-sulfates) in external mixtures of particles with diameter as small as 8 nm [*Väkevä et al.*, 2002; *Swietlicki et al.*, 2008]. TDMA studies suggest that nss-sulfates dominate the ambient, sub-100 nm diameter, marine aerosol outside the surf zone [*Berg et al.*, 1998; *Fletcher et al.*, 2007; *Swietlicki et al.*, 2008; *Allan et al.*, 2009; *Good et al.*, 2010b]. A more scarce externally mixed SSA component is also observed [*Berg et al.*, 1998; *Fletcher et al.*, 2007; *Swietlicki et al.*, 2008]. When SSA are observed, they comprise 11-40% of the sub-165 nm number fractions at Mace Head, Ireland (North Atlantic) [*Bialek et al.*, 2012], 11-14% of the sub-100 nm number fractions in the West Atlantic [*Swietlicki et al.*, 2000], 12-15% in the Pacific [*Berg et al.*, 1998] , 23% in the open Southern Ocean [*Berg et al.*, 1998] and 1-15% at Cape Grim, Australia (Southern Ocean) [*Gras and Ayers*, 1983; *Fletcher et al.*, 2007] An exception to this pattern is the very high proportions of sub-100 nm SSA (95-100%) observed in the Arctic, but only in 3-7% of all measurements at 35 and 50 nm [*Zhou et al.*, 2001].

The Southern Ocean is a particularly interesting region for SSA due to the higher than global average wind speeds and thus strong potential for SSA production. Further observations of

100 the marine aerosol at Cape Grim using electron microscopy and X-ray spectroscopy of
101 individual particles identify number fractions of SSA of 5-25% in the 50-150 nm size range.
102 These fractions correspond to SSA number concentrations of the order of 30 to 100 cm^{-3}
103 [*Murphy et al.*, 1998a; 1998b]. Values for the open Southern Ocean range from 1 to 150 cm^{-3}
104 for particles greater than 80 nm diameter [*Bates et al.*, 1998; *Kreidenweis et al.*, 1998;
105 *Murphy et al.*, 1998b; *Lewis and Schwartz*, 2004]. Observations of sub-100 nm SSA in the
106 Southern Ocean are sparse and studies report widely varying SSA concentrations, from 1 to
107 171 cm^{-3} [*Bates et al.*, 1998; *Kreidenweis et al.*, 1998; *Murphy et al.*, 1998b; *Lewis and*
108 *Schwartz*, 2004]. Further observations of sub-100-nm SSA particles are required to assess
109 the importance of the Southern Ocean as a source of SSA and thus CCN.

110 The chemical composition of SSA under different oceanic and meteorological conditions is
111 also an active area of research. It is known that nascent SSA is comprised of internally and
112 externally mixed inorganic (sea salt) and organic fractions. Table 1 summarises results from
113 some recent studies, which examined the composition of nascent SSA. TDMA analyses of
114 laboratory generated SSA particle composition reveals internally mixed organic mass
115 fractions on the order of 5-27% for sub-200 nm particles [*Modini et al.*, 2010; *Fuentes et al.*,
116 2011]. Off-line chemical composition measurements of ambient [*O'Dowd et al.*, 2004;
117 *Rinaldi et al.*, 2010] and laboratory generated [*Keene et al.*, 2007; *Facchini et al.*, 2008] SSA
118 particles have identified much larger organic fractions of up to 80% for sub-200 nm particles
119 in the North Atlantic. Ambient TDMA observations in the North Atlantic (Mace Head)
120 displayed externally mixed non-hygroscopic particles, consistent with primary organics with
121 a small sea salt component, contributing up to 75% of the Aitken mode ambient particle
122 number [*Ovadnevaite et al.*, 2011]. Flux measurements [*Ceburnis et al.*, 2008] and an
123 increasing ambient organic mass with decreasing particle size [*O'Dowd et al.*, 2004; *Facchini*

124 *et al.*, 2008] have provided evidence that the large observed organic fraction is predominantly
125 primary, with a relatively small contribution from secondary organics.

126 Primary marine organics have also been observed using particle analysis by laser mass
127 spectrometry at Cape Grim [*Middlebrook et al.*, 1998; *Murphy et al.*, 1998a]. These authors
128 argued that a small sodium sulfate fraction in these particles and the presence of iodine,
129 which was correlated with organic concentrations, indicated relatively freshly emitted SSA.
130 This is consistent with simultaneous depletion of iodine and chlorine and accumulation of
131 sodium sulfate from the marine boundary layer observed at Cape Grim, which suggest a
132 primary iodine source [*Murphy et al.*, 1997]. Average organic mass fractions in SSA were
133 approximately 10% for particles between 1.6 and 3 μm in diameter [*Middlebrook et al.*, 1998;
134 *Murphy et al.*, 1998a]. This organic mass fraction was variable ranging from 5 to 50% and
135 authors suggest it may have been enhanced at the lower end of the observed size range, ~170
136 nm. These results are broadly consistent with observations of a residual component, the
137 difference between the ionic and gravimetric mass, which comprised 21% (0.23 $\mu g/m^3$) of the
138 Southern Hemisphere mid-latitudes submicron mass [*Quinn et al.*, 2000]. A submicron
139 carbon mass concentration of 0.23 $\mu g/m^3$ was also observed via proton elastic scattering
140 analysis at Cape Grim, suggesting a similar organic component [*Andreae*, 1982].

141 Adsorption theory predicts that during rough sea conditions the enhanced concentration of
142 surfactant organic matter at the ocean surface saturates the SSA adsorption process. A
143 surfactant organic matter film of approximately the same thickness develops on SSA
144 independent of particle size and will therefore form increasing fractions of total particle
145 volume as particle size decreases [*Oppo et al.*, 1999]. The majority of size-resolved SSA
146 organic volume or mass fraction measurements have supported this theory through the
147 observation of increasing primary organic fractions in SSA with decreasing particle size

148 [*O'Dowd et al.*, 2004; *Rinaldi et al.*, 2009; *Quinn et al.*, 2014]. However, this trend has not
149 been observed in all experiments [*Modini et al.*, 2010].

150 Externally mixed organics have also been explicitly identified in SSA. X-ray analysis of
151 transmission electron microscopy (TEM) samples and single particle mass spectrometry
152 measurements for ambient marine and wave chamber aerosols have indicated external
153 mixtures. These external mixtures are dominated by organics with contributions from organic
154 particles to the overall sub-100 nm particle population, ranging from approximately 80 to
155 100% [*Bigg and Leck*, 2008; *Leck and Bigg*, 2010; *Prather et al.*, 2013]. Of particular note
156 are the ambient observations from Cape Grim, which are characterized by an absence of sea
157 salt in the sub-100 nm particle fraction. These particles are hypothesised to be primary
158 particles from the sea surface microlayer [*Bigg*, 2007; *Leck and Bigg*, 2010]. A small fraction
159 of individual 0.2 to 2μm, externally mixed bacterial cells have also been identified in TEM
160 samples over the Southern Ocean [*Pósfai et al.*, 2003].

161 A seasonal trend has been observed in the organic enrichment of SSA particles at Mace Head,
162 with higher organic fractions thought to be largely comprised of a primary organic fraction,
163 observed during the biologically active summer months [*O'Dowd et al.*, 2004]. However,
164 recent research suggests the ever-present pool of oceanic dissolved organic matter (DOM),
165 composed primarily of saccharides, proteins and processed, recalcitrant organic molecules,
166 provides sufficient matter for organic enrichment of SSA to occur even in non-productive
167 regions [*Burrows et al.*, 2014; *Quinn et al.*, 2014]. These studies and the observations of high
168 internally and externally mixed organic fractions in small SSA particles lead to the
169 suggestion that organics will dominate sub-100 nm SSA composition in most oceanic
170 conditions. This raises questions about the importance of sea salt in sub-100 nm SSA. The
171 previously mentioned TDMA studies indicate externally mixed SSA with large by sea salt
172 fractions, however the precise organic fraction of the SSA component is unknown [*Berg et*

173 *al.*, 1998; *Fletcher et al.*, 2007; *Swietlicki et al.*, 2008]. In addition recent cloud level studies
174 in pristine conditions also identify sea salt particles down to 40 nm in diameter from
175 atmospheric and in-droplet sampling using TEM [*Twohy et al.*, 2013] and volatility
176 techniques [*Blot et al.*, 2013]. These observations provide an indication that sub-100nm sea
177 salt plays a role in marine cloud formation.

178 Here we present observations from a unique, short lived and particularly strong SSA event,
179 which occurred in clean Southern Ocean air masses over 2 days in summer 2007 at the Cape
180 Grim Baseline Air Pollution Station (BAPS) on the north-west tip of Tasmania, Australia.
181 We use aerosol hygroscopicity and volatility measurements to identify sub-100nm SSA
182 composition and discuss the conditions under which this SSA was produced and transported
183 to Cape Grim. The case study does not necessarily provide an indication of the long-term
184 average sub-100 nm aerosol composition at Cape Grim. This unique SSA event was selected
185 as a case study because it contributes to our understanding of the chemical composition of
186 sub-100 nm ambient SSA and the factors that control SSA concentrations in the atmosphere.

187 **2. Experimental methods**

188 **2.1. Cape Grim Baseline Monitoring Station**

189 From 22 November 2007 to 11 December 2007 aerosol observations were undertaken at the
190 Cape Grim BAPS on the north-west tip of Tasmania, Australia. These observations were
191 aimed at examining the properties of the naturally occurring marine aerosol. Here we focus
192 on measurements taken from 7 – 8 December, when a particularly strong SSA event was
193 observed from the station.

194 The Cape Grim BAPS is situated 94 m above sea level, well located for examining clean air
195 from the Southern Ocean. Winds from the south-west, the baseline sector (190° to 280°),
196 typically traverse across several thousand km of the Southern Ocean [*Gras*, 2009]. Modelling
197 of air flow around the Cape Grim station indicates that sampling from the 10 m inlet (104
198 metres from sea level) delivers air with a source height over the near ocean ranging from 10
199 to 30 m, when the air is from the baseline sector, suggesting that observations are unlikely to
200 be influenced by local sources such as wave breaking [*Baines and Murray*, 1994]. In addition
201 to the wind direction a minimum wind speed of 7 km/hr (1.94m/s) was used in this study to
202 determine baseline conditions, this is consistent with previous aerosol monitoring at Cape
203 Grim [*Gras*, 2009]. Total particle number and radon concentrations are also commonly used
204 as indicators of baseline conditions in Cape Grim and these measurements are reported along
205 with our results.

206 **2.2. Instrumentation**

207 Total aerosol concentrations were measured using two condensation particle counters
208 (CPCs), a TSI 3010 and 3025 (TSI, Shoreview, MN). The 3010 CPC has a detection size
209 limit of 10 nm at the lower end of its range, while the 3025 has a detection size limit of 3 nm.
210 The number of 3-10 nm diameter particles can be obtained from the difference in the
211 concentrations reported by these two instruments providing information on the concentration
212 of nucleation mode particles. Aerosol size distributions from 15 to 737 nm were obtained
213 using a scanning mobility particle sizer, consisting of a TSI 3071 Differential Mobility
214 Analyser and TSI 3776 CPC. Black carbon concentrations, inferred from light absorption,
215 and radon concentrations were measured as markers for continental air and pollution at a time
216 resolution of 60 min. Details of light absorption and radon measurements at Cape Grim can
217 be found in *Gras* [2011] and *Zahorowski et al.* [2004].

Further aerosol properties and compositional information were obtained with a custom-built VH-TDMA [*Johnson et al.*, 2004]. The VH-TDMA is a particle sizing instrument that selects particles based on mobility diameter, conditions them, and then measures the resulting particle size distributions using two parallel scanning mobility particle sizers (SMPS), each with a TSI 3010 CPC. The temperature difference between the saturator and the condenser was set to 21°C in both 3010 CPCs and the counting efficiencies updated accordingly to extend the lower size limit of the CPCs down to 5nm diameter [*Mertes et al.*, 1995]. The VH-TDMA combines humidification and volatilisation conditioning to examine hygroscopic properties of the aerosol fraction remaining after volatilisation. It can be used to distinguish between two components of sub-micron heterogeneously mixed particles, and is especially useful in distinguishing between components displaying significantly different hygroscopic properties [*Johnson et al.*, 2004]. The VH-TDMA provides valuable information on the mixing state of marine particles, which is of particular interest with recent studies highlighting the importance of externally mixed organics [*Leck and Bigg*, 2005b; 2010; *Collins et al.*, 2013; *Prather et al.*, 2013].

The VH-TDMA measured sub-100 nm mode particles and was run in several operating modes:

1. Volatility mode. For a fixed preselected particle size the humidity was kept constant at relative humidity (RH) 90% and the temperature of the thermodenuder was scanned from room temperature to 280°C. During this mode the particle volume fraction remaining (VFR) can be calculated from the first SMPS using:

$$VFR = \frac{d_T^3}{d_i^3}$$

Where d_T is the particle diameter at temperature, T and d_i is the initial particle dry diameter. The growth factor (VH-GF) observed by the second SMPS is due to both volatility and hygroscopic growth and is given by:

$$VH - GF = \frac{d_{90,T}}{d_i}$$

Where $d_{90,T}$ is the particle diameter after being exposed to 90%RH and passing through the thermodenuder set to temperature, T. Changes in the HGF observed during this temperature scan can result from the evaporation of non-refractory components in the thermodenuder (e.g. organics, sulfate).

2. H-TDMA mode. When the thermodenuder was kept at room temperature the instrument operated as a standard H-TDMA. In H-TDMA mode two further modes of operation were utilised: 1) HGF mode where the instrument was operated at fixed 90% RH, and 2) deliquescence mode where the RH was ramped from 60 to 90% in steps as small as 0.5% [*Johnson et al.*, 2008]. Deliquescence curves provide clearer differentiation between different inorganic salts (e.g. ammonium sulfate and sodium chloride) and internally mixed inorganic-organic particles than is possible from HGF measurements at a single RH.

2.3. Data analysis procedures

The HGF is defined as the ratio of humidified particle diameter to dry particle diameter and is commonly measured at 90% RH. HGF provides information on particle composition [*Berg et al.*, 1998; *Zhou et al.*, 2001; *Swietlicki et al.*, 2008]. Previous studies have generally partitioned the marine sub-100 nm aerosols into four HGF classes, used to provide guidance on what chemical species are likely to be present in the aerosol. The aerosol composition is inferred from the known HGFs of common species [*Tang and Munkelwitz*, 1994] and H-TDMA field data [*Swietlicki et al.*, 2008].

1. Nearly hydrophobic aerosols, with growth factors ranging from approximately 1.0 to 1.1, are composed of marine organics or are influenced by anthropogenic sources [*Berg et al.*, 1998; *Swietlicki et al.*, 2000; 2008; *Bialek et al.*, 2012].
2. Less hygroscopic aerosols, with growth factors ranging from approximately 1.1 to 1.3, are often composed of marine organics [*Ovadnevaite et al.*, 2011; *Bialek et al.*, 2012].
3. More hygroscopic aerosols, with growth factors ranging from approximately 1.35 to 1.85, are commonly dominated by nss-sulfates [*Swietlicki et al.*, 2000; *Ovadnevaite et al.*, 2011; *Bialek et al.*, 2012].
4. Sea salt aerosols (inorganic SSA), with growth factors of more than 1.85, observations of sub-100 nm sea salt is not common and the ideal conditions for their development is uncertain [*Zhou et al.*, 2001; *Fuentes et al.*, 2010; *Modini et al.*, 2010; *Bialek et al.*, 2012].

Inferring chemical composition purely from particle HGFs can be problematic since different internal mixtures can result in the same HGF. For example, sea salt and sulfate particles could both be classified in the more hygroscopic class when internally mixed with less hygroscopic material. In this study HGFs are examined alongside particle volatility and deliquescence data, providing a more complete picture of particle composition and mixing state.

All VH-TDMA data were inverted using the TDMAinv algorithm [*Gysel et al.*, 2009]. The resulting growth factor probability distributions were used to determine the median HGF for each mode. The 95% confidence interval in the median or the experimental uncertainty of ±3% [*Modini et al.*, 2010], whichever value was greater, was applied to represent the uncertainty. Uncertainties ranged from ±3% at between 22 and 55 nm to ±6% at 16 nm. To estimate the change in CCN concentration with changing particle composition, the κ

parameter was calculated using the measured HGFs for a range of particle diameters [*Petters and Kreidenweis*, 2007]. A critical dry diameter, beyond which particles are activated as CCN, for each super-saturation was calculated and size distributions used to determine the fraction of particles exceeding the critical diameter.

2.4. Back trajectory analysis

The Hybrid Single Particle Lagrangian Integrated Trajectory (HYSPLIT) model [*Draxler and Rolph*, 2013] was used to identify the air mass properties associated with observations of high SSA concentrations. These back trajectories were computed using meteorological data from the NOAA/NCEP Global Data Assimilation System (GDAS) [*Kanamitsu*, 1989]. Using HYSPLIT we obtained 7-day back trajectories for each hour of the campaign, these were compared to particle measurements at Cape Grim, particularly SSA concentrations. Of interest in the baseline sector was the modelled back trajectory altitude, relative humidity, rainfall and mixing height. 6 hourly surface wind speed data observed from the Cross-Calibrated Multi-Platform (CCMP) data set were extracted along the back trajectories. The CCMP data set includes cross-calibrated satellite winds derived from a variety of satellite instrumentation on a 0.25° grid e.g. QuikSCAT, SeaWinds, Windsat [*Atlas et al.*, 2013].

In addition the UK Met Office Numerical Atmospheric-dispersion Modelling Environment (NAME) was used to create back trajectory probability plots and ensure clean marine background air origin [*Jones et al.*, 2007].

3. Results and Discussion

3.1. Event characterisation

Size distribution data from the 7 – 8 December 2007 indicate there was a developing accumulation mode from 13:00 to 15:00 on 7 December, coincident with enhancement of an Aitken mode, resulting in an increase in total particle concentrations from approximately 450 to 900 cm^{-3} (Figure 1). Following this a bimodal marine aerosol size distribution was observed [*Sellegri et al.*, 2001; *Lewis and Schwartz*, 2004; *Heintzenberg et al.*, 2011] containing a larger Aitken mode, initially with a peak at 23 nm, and an accumulation mode with a peak at 145 nm. This suggests previous cloud processing of the aerosol had occurred, with those particles over 70 nm having previously been activated and readily growing into the accumulation mode, whilst smaller particles remained inactivated leading to a Hoppel minimum at 70 nm [*Hoppel et al.*, 1986]. On 8 December, the peak of the Aitken mode grew slowly from approximately 23 nm in the morning to approximately 60 nm at 18:00. Total particle concentrations increased substantially after 10:00 (Figure 1), primarily driven by an increase in the concentration of 3 – 10 nm nucleation mode particles. These particles may have contributed to the Aitken mode growth observed in the afternoon on 8 December through coagulation.

Modelled back trajectories show a clean, Southern Ocean origin for air masses arriving at Cape Grim during the period from 19:00 7 December to 07:00 8 December (Figure 2). Local wind speed and direction at Cape Grim from 12:00 7 December to 06:00 8 December were also indicative of air masses arriving almost entirely from the clean marine sector (Figure S4) [*Gras*, 2009]. After 06:00 local wind direction shifted slightly north resulting in intermittent baseline conditions. By 10:00 baseline conditions had finished completely. Consistent with the local meteorological data at 07:00 – 10:00 8 December there was a slight shift in the path

of the modelled back trajectories demonstrating the air mass came closer to the Australian mainland near the major city of Melbourne. From 12:00 7 December to 18:00 8 December black carbon concentrations ranged from 1.3 to 10 ngm^{-3}, and radon concentrations ranged from 27 to 80 $mBqm^{-3}$, which is consistent with the values observed for baseline periods at Cape Grim [*Zahorowski et al.*, 2011].

Entrained particles from the free troposphere are a possible cause of the increases in particle concentrations observed on 8 December. This is consistent with previous studies at Cape Grim by [*Gras et al.*, 2009], where peaks in the concentration of 3-10nm particles were observed following the passage of cold fronts. Gras and co-workers have convincingly argued the concentration enhancements are due to nanoparticle-rich free tropospheric air rapidly mixing to the surface in the turbulent postfrontal atmosphere. Enhancements of approximately 100 cm^{-3} and peaks of 300-500 cm^{-3} are typically observed 9—11 hours after the passage of a front, and are separated by 8-11 hour intervals. Synoptic charts (Figure S6) and observed pressure (Figure S3) indicate that a cold front passed Cape Grim at approximately 05:00 7 December. Immediately following the front concentrations of 3-10 nm particles were initially greater than 150 cm^{-3} due to continental influences. By 11:00 the wind direction settled into the baseline sector and concentrations were low, 50 cm^{-3}. Hourly average nanoparticle concentrations of 70 to 170 cm^{-3} occurred from 15:00 7 December until 10:00 on 8 December, consistent with the postfrontal observations by [*Gras*, 2009]. Sharp increases in concentration to peaks above 1000 cm^{-3} were observed after 10:00 8 December. These enhancements are larger and sharper than those previously observed in postfrontal conditions at Cape Grim. The sharp concentration peaks correspond with the end of baseline conditions as defined by wind speed and direction and the shifting of the air mass trajectory closer to the major city of Melbourne, which suggests that they could be the result of intermittent intrusions of anthropogenically-influenced air. Despite the sharp increases in

nucleation mode particle concentrations radon and black carbon concentrations remained low until approximately 18:00. This is potentially because the lower time resolution black carbon and radon measurements failed to capture the sharp, intermittent concentration increases. After 18:00 8 December particle, black carbon and radon concentrations (Figure S1) all increased signifying the complete establishment of polluted conditions at Cape Grim.

3.2. Hygroscopic growth factors

The VH-TDMA was run mainly in the H-TDMA mode during the 7 – 8 December event. Observations of sub-100 nm particle hygroscopicity at 90% RH from the afternoon of 7 December (16:30) to the afternoon of 8 December (15:00) indicate an external mixture of at least two distinct types of aerosols, one in the more hygroscopic mode with raw growth factor of 1.45 to 1.65, and another in the sea salt mode with growth factor 1.95 to 2.1 (see Figure 3A and Figure S5). HGF corrections due to shape and Kelvin effects are described in the remainder of this section. The observed HGFs are consistent with an external mixture of predominantly nss-sulfates and SSA. These will subsequently be referred to as the nss-sulfate and SSA modes, respectively. Strong justification for these mode assignments is presented in the following sections.

The HGF probability distribution (Figure S5) was used to estimate the number fraction of particles in each mode. Figure 1C shows the time series of the SSA mode number fraction. Small fractions of externally mixed sea salt were initially observed between 15:00 and 16:30 7 December. By approximately 05:30 on 8 December SSA number fractions reached as high as 69%. The increase in the proportion of the SSA mode (15:00 7 December to 05:30 8 December) coincided with postfrontal enhancements in nanoparticle concentrations (section 3.1). The number fraction of SSA particles decreased after 06:00 8 December, corresponding with a shift in wind direction signalling intermittent baseline sector measurements. After

10:00 baseline conditions had ended completely and after 18:00 no SSA particles were observed. During the peak of this event SSA particle number fractions were variable but almost exclusively greater than 0.2.

When the SSA mode fraction reached its maximum value measurements of the HGF at different sizes were conducted between 7:30 and 8:40 on 8 December. Considerable fractions (24-50%) of SSA particles were detected at all particle sizes examined between 16nm and 97 nm diameter. Figure 3A shows the HGF of the two modes as a function of particle size as well as the Kelvin and shape corrected HGFs for both modes. Freshly emitted SSA has a non-spherical shape and can be described with the NaCl shape correction factor [*Niedermeier et al.*, 2008; *Wise et al.*, 2009; *Modini et al.*, 2010]. SSA can become more spherical via atmospheric processing [*Laskin et al.*, 2012] and a higher organic content [*Laskin et al.*, 2012; *Ault et al.*, 2013]. In this study a case with no shape factor adjustment (i.e. spherical SSA), and a case with a size dependant shape-factor for NaCl, ranging from 1.20 to 1.23, was applied to the SSA mode to provide a lower and upper limit for the HGF of the SSA. A constant shape factor of 1.02 was applied to the sulfate mode [*Biskos et al.*, 2006b; 2006c]

In addition, for the comparison of HGFs across particles of different sizes the influence of the Kelvin effect had to be negated. This was achieved by converting HGFs measured at 90% RH to bulk growth factors (i.e. where water activity = RH = 90%) using a single parameter representation of hygroscopic growth, κ [*Petters and Kreidenweis*, 2007]. The Kelvin corrected, and shape and Kelvin corrected HGFs are referred to as 'K corrected' and 'K/shape corrected' HGFs in Figure 3A.

The Kelvin corrected HGF for the SSA particles, without shape factor correction, ranged from 2.05 ± 0.09 at 95 nm to 2.3 ± 0.1 at 16 nm. The measured Kelvin and shape corrected HGF for the SSA mode ranged from 2.3 ± 0.1 at 95 nm to 2.5 ± 0.2 at 16 nm. Kelvin and

405 shape corrected HGFs for 16 nm SSA and nss-sulfate particles exceeded the HGFs for
406 artificial SSA and laboratory $(NH_4)_2SO_4$, respectively. This suggests that the ambient
407 particles were more spherical than laboratory analogues. Overnight HGFs were higher than
408 observed during size resolved measurements on the morning of 8 December (triangle
409 compared to circle markers Figure 3A), this may indicate a change in the SSA morphology.

410 Assuming that the suppression of the Kelvin corrected SSA HGFs (without shape factor
411 correction) is entirely due to the presence of an internally mixed organic component, an upper
412 bound for the organic volume fraction can be calculated via the Zadanovkii-Stokes-Robinson
413 (ZSR) assumption [*Stokes and Robinson*, 1966; *Chen et al.*, 1973]. ZSR calculation were
414 made using measured SSA HGFs (without shape factor correction), an artificial sea salt HGF
415 of 2.35 and a HGF for the organic fraction of 1 and 1.5 [*Peng et al.*, 2001; *Gysel et al.*, 2004;
416 *Mikhailov et al.*, 2004; *Fuentes et al.*, 2011]. Assuming an organic growth factor of 1, the
417 average sub-100 nm organic volume fraction was 26%, ranging from 11% at 16 nm to 37% at
418 95 nm. An assumed organic growth factor of 1.5 yielded an average sub-100 nm organic
419 volume fraction 33%, ranging from 14 to 46%.

420 Alternatively aging of the SSA could have enhanced the sulfate component to the detriment
421 of more hygroscopic species such as NaCl. Thus, the suppression of HGFs relative to
422 artificial sea salt is possibly due to an ambiguous combination of inorganic sea salt ageing
423 and the presence of both primary and secondary organic components. Therefore, the 11 –
424 46% SSA organic volume fractions should be considered as upper limit estimates.

425 **3.3. SSA number concentrations**

426 The size dependent SSA number fractions observed between 7:30-8:40 am 8 December were
427 multiplied by the average total aerosol size distribution during this time period to estimate the

SSA size distribution up to 100 nm diameter, (Figure 3B). Lower and upper bound estimates of the SSA size distribution were derived based on the range of total particle concentrations (284 - 363 cm^{-3}) and SSA number fractions (at the single particle size at which most measurements were taken, 95 nm, 26 – 49 %) measured during the time period 7:30 to 8:40. The lower and upper bound size distribution estimates correspond to integrated sub-100 nm SSA particle concentrations of 41 and 109 cm^{-3}, respectively.

The integrated sub-100 nm SSA concentrations estimated for the period 7:30 – 8:40 8 December were scaled by measured SSA number fractions (Figure 1C) to estimate integrated sub-100 nm SSA particle concentration over the entire 2-day event (Figure 1E). This scaling procedure assumes that the shapes of the SSA and total particle size distributions were constant from 7 – 8 December, which is not strictly true (Figure 1A), so these calculated concentrations should be considered as approximate estimates only. The peak SSA number fraction of 0.69 observed at approximately 05:30 8 December corresponds to sub-100 nm SSA particle concentration in the range 110 – 290 cm^{-3}.

3.4. Volatility

To further confirm that the observed highly hygroscopic particles were SSA with a large sea salt fraction the VH-TDMA was run in volatility mode from 9:10 to 10:15 on 8 December. A particle size of 56 nm was preselected and the temperature of the thermodenuder was ramped from room temperature to 280°C. The VFR and VH-GFs at 90% RH of the non-volatile particles remaining at each temperature step were examined. The number fraction of the SSA mode during this period was up to 0.4 based on the HGF probability distribution. The VFR showed a population of particles evaporating at 160-200°C. This corresponded with a reduction in the VH-GF of particles in the more hygroscopic mode (HGF 1.5) (Figure 4). This combined volatility and hygroscopic behaviour closely matches that observed for

laboratory generated ammonium sulfate [*Fletcher et al.*, 2007; *Swietlicki et al.*, 2008], which is also displayed in Figure 4. At 280°C particles in the SSA mode had a VFR of 0.90 ± 0.05, the VFR of artificial SSA at this temperature is 0.93 ± 0.03 [*Modini et al.*, 2010]. This, in combination with the very high HGF, is strong evidence for SSA with a very small volatile organic or enhanced sulfate fraction, but does not exclude the presence of non-volatile organics (Figure 4).

3.5. Deliquescence

Dependence of the HGF on relative humidity was examined by two separate deliquescence scans conducted between 22:00 7 December and 00:00 8 December. During this period the number fraction of SSA mode particles was up to 0.15 (Figure 1). Three distinct populations of particles were observed in the deliquescence scans (Figure 5), For one group of particles there was a prompt increase in growth factor to 1.8 at 73-75% RH. This is consistent with the deliquescence of sea salt [*Berg et al.*, 1998; *Biskos et al.*, 2006a]. Furthermore, the HGFs above 75% RH of these particles closely matched those of modelled and measured sodium chloride and sea salt [*Fletcher et al.*, 2007], as already discussed above with reference to the continuous HGF measurements at 90% RH. The deliquescence, volatility and growth factor of this mode provides compelling evidence that it is SSA, with a large (>50% by volume) inorganic sea salt component.

For another group of particles reasonably prompt deliquescence was observed at approximately 78-80% RH, which matches the deliquescence RH of ammonium sulfate [*Biskos et al.*, 2006b; *Fletcher et al.*, 2007]. In addition the HGF for this mode above 79% RH closely matched that modelled for ammonium sulfate [*Fletcher et al.*, 2007]. The third group of particles did not display prompt deliquescence and was characterised by a continuous increase in growth factor from 1.3 at 65% RH to 1.4 at 80 % RH. This behaviour

476 is consistent with nss-sulfates containing an ammonium to sulfate ratio less than that for
477 ammonium sulfate, referred to as partially neutralised nss-sulfates. One such nss-sulfate is
478 ammonium bisulfate, which has a deliquescence RH of 40% RH [*Tang and Munkelwitz*,
479 1994; *Fletcher et al.*, 2007].

480 There was a distinct increase in the proportion of ammonium sulfate to the detriment of the
481 partially neutralised sulfate fraction over the time between the two deliquescence scans,
482 shown in Figure 5. Additional growth factor measurements at 74-76% RH were used to
483 separate the partially neutralised sulfate and ammonium sulfate, and to calculate the number
484 fraction of partially neutralised nss-sulfates. These number fractions are shown in Figure 1D.
485 At 12:00 7 December the aerosol was composed entirely of partially neutralised sulfate
486 particles. Between 18:00 and 00:00 the fraction of partially neutralised nss-sulfates decreased
487 from 0.6 to 0 (Figure 1). At 15:00 nanoparticle concentrations increased and sparse HGF
488 measurements indicate that the SSA was first observed between 15:00 and 22:00. This
489 suggests that the ammonia, SSA and nucleation mode particles all arrived in the same air
490 mass.

491 **4. Implications**

492 Hygroscopic growth, volatility and deliquescence measurements of sub-100 nm ambient
493 marine particles at Cape Grim during this event identified high concentrations of SSA with a
494 large proportion of inorganic salts (greater than 50% by volume) down to 16 nm in diameter.
495 The SSA number fraction reached a maximum of 0.69 early on 8 December 2007, which
496 corresponds to sub-100 nm SSA concentrations of 110-290 cm^{-3}. The full SSA size
497 distribution most likely peaks at a diameter greater than 100 nm [*Prather et al., 2013; Lewis*
498 *and Schwartz, 2004*]. Therefore total SSA concentrations were likely substantially higher
499 than the sub-100 nm SSA concentrations reported here. Previous observations in the Southern

500 Ocean have observed SSA concentrations for particles greater than 80 nm in diameter of up
501 to 170 cm^{-3} [*Kreidenweis et al.*, 1998]. High SSA concentrations will enhance CCN
502 concentrations, with possible climate implications.

503 **4.1. Sea spray composition**

504 Very few ambient marine observations are characterised by sub-100 nm SSA fractions of
505 greater than 0.5, with measurements particularly scarce in the Southern Hemisphere (Table
506 2). Previous summertime studies of ambient SSA in the north Atlantic [*O'Dowd et al.,* 2004]
507 and *in situ*, artificially produced SSA in the north Pacific [*Quinn et al.,* 2014], observed an
508 increasing SSA organic fraction, up to approximately 80%, with decreasing particle size . The
509 ambient SSA organic fraction was identified as predominantly primary, however did contain
510 a secondary organic component [*O'Dowd et al.*, 2004; *Ceburnis et al.*, 2008]. Results from
511 our study are not consistent with relationships observed in *O'Dowd et al.* [2004] and *Quinn et*
512 *al.* [2014]. Contrary to the above studies the observed organic volume fraction from the HGF
513 measurements was up to 11 – 46 %, and increased HGFs with decreasing particle sizes down
514 to 16 nm in diameter suggested a decreasing organic fraction. The results herein are broadly
515 consistent with submicron organic mass fractions of 5-50% previously observed in the
516 Southern Ocean [*Quinn et al.*, 2000; *Middlebrook et al.*, 1998; *Murphy et al.*, 1998a;
517 *Andreae*, 1982]. Other studies looking at sub-100 nm SSA artificially produced in-situ in the
518 North Pacific [*Bates et al.*, 2012], have observed a HGF suppressed by 10% relative to
519 artificial sea salt and independent of the particle size. SSA observed in this study displayed
520 similarly suppressed HGFs and were also non-volatile (to 280 °C), suggesting that if there are
521 any internally mixed organic components they were non-volatile. This study provides a
522 unique characterisation of hygroscopic and volatile properties of summertime sub-100 nm
523 SSA with a dominant (greater than 50%) inorganic component.

524 TEM images of 50nm particles collected between 08:00 and 16:00 8 December 2007 are not
525 consistent with sea salt or ammonium sulfate and resemble organic particles thought to be
526 from the surface ocean microlayer [*Leck and Bigg*, 2010]. These particles appeared to be
527 made up of aggregates of 5 nm particles held together in a transparent matrix [*Leck and Bigg*,
528 2010]. In addition high resolution X-ray spectrometry of particles during this period
529 identified calcium as the element detected with the highest concentration, along with sulfur.
530 Sodium was near absent in the TEM-samples indicating that little to no sea salt was present
531 [*Leck and Bigg*, 2010]. A similar composition was observed by the same authors in other
532 oceans using the same methodology [*Leck and Bigg*, 2005a; *Bigg and Leck*, 2008; *Leck and*
533 *Bigg*, 2008]. The chemical composition, both in terms of the organics observed but even
534 more important in terms of the inorganic composition, reported by [*Leck and Bigg*, 2010], is
535 in contrast with the observations herein. We have shown clear evidence of a large fraction
536 (~50%) of highly hygroscopic (HGF~2), refractory (up to 280°C) sub-100 nm particles that
537 deliquesced around 74% RH. This combination of properties provides unambiguous evidence
538 of the presences of large numbers of sub-100 nm SSA with a large proportion (greater than
539 54% by volume) of inorganic salts. It is unclear whether the absence of sea salt in TEM
540 samples resulted from misattribution of sea salt due to the presence of a non-volatile organic
541 component or an absence of sea salt particles resulting from inadequate sampling statistics
542 (only 10 particles sampled on 8 December 2007 are discussed by *Leck and Bigg* [2010]; 4
543 imaged by TEM, and 6 analysed by X-ray spectrometry). These results bring into question
544 the applicability of TEM data to provide quantitative and representative data on the
545 composition of atmospheric aerosols, and could have consequences for observations in other
546 ocean basins.

547 Observations of primary marine aerosols have been undertaken using a wide range of
548 techniques and indicate great spatial and seasonal variation in composition. Simultaneous

549 measurements using online and offline methods are rare and this study highlights the
550 potential for biases in analysis techniques to influence marine aerosol measurements, which
551 are already complicated by spatial and seasonal variations. Further inter-comparison studies
552 are needed to appropriately quantify the composition of sub-100 nm SSA.

553 **4.2. SSA source**

554 Air mass back trajectories for periods during which the highest proportion of SSA were
555 observed at Cape Grim were characterised by relatively high altitude, and thus low pressure
556 and temperature, as well as low relative humidity and rainfall (Figure 6). There were two
557 high surface wind speed periods in the back trajectories spanning the high SSA event. The
558 first was 20-40 hours preceding the arrival of the air mass at Cape Grim and involved wind
559 speeds of 10.2 - 19.9 ms^{-1}. The second was approximately 100 hours upwind of Cape Grim
560 and involved wind speeds of 12 - 18.5 ms^{-1}. The high surface wind speed periods correspond
561 to locations approximately 1500 km and 3200 km west and south-west of Cape Grim,
562 respectively. Ocean surface wind speeds were similar for back trajectories from 15:00 7
563 December to 17:00 8 December, suggesting that the SSA production was relatively constant
564 for these back trajectories.

565 Peak SSA concentrations corresponded with a minimum in atmospheric turbulence at Cape
566 Grim, the boundary layer depth falling from 1060 m at 17:00 on 7 December to 650 m at 4:00
567 on 8 December. This indicates that the relatively constant source of SSA was ejected into an
568 increasingly compressed boundary layer, which resulted in increased SSA concentrations
569 from 7:00 on 7 December to 4:00 on 8 December. Following this the boundary layer rose and
570 the SSA concentrations dropped again. Back trajectories corresponding to the highest SSA
571 fractions had periods above the boundary layer, particularly from 110 to 140 hours before the

572 air mass reached Cape Grim (Figure 6). This suggests that the arrival of air masses with high
573 SSA concentrations at Cape Grim coincided with sulfates from the free troposphere.

574 There was no precipitation associated with the high surface wind event 1500 km west of
575 Cape Grim. This supports cloud level measurements in the Pacific where increased SSA
576 production during high wind speed events were observed to be offset by even modest
577 increases in precipitation [*Blot et al.*, 2013].

578 **4.3. Contribution to CCN**

579 Meteorological observations, back trajectory modelling and nanoparticle measurements all
580 indicate that increased SSA concentrations were associated with entrainment of air from the
581 free troposphere. The size distribution of particles over the period when SSA was observed
582 indicates the presence of a Hoppel minimum at 63 to 82 nm (Figure 3B). The Hoppel
583 minimum is apparent in the total aerosol size distributions, but is unclear in the SSA size
584 distributions (Figure 3B). Although it is unclear whether there were SSA particles that were
585 previously activated into cloud droplets, the high measured HGFs indicate that the SSA
586 particles could make a contribution to the cloud level CCN in this region during periods with
587 sufficient updraft velocity.

588 To examine the enhancement of CCN concentrations due to the high SSA fractions observed
589 during the SSA event sub-100 nm HGFs were used to estimate single hygroscopicity
590 parameters (κ) for both the SSA and nss-sulfate modes [*Petters and Kreidenweis*, 2007]. The
591 κ parameters were then used to calculate CCN concentrations at 25°C. Two cases were
592 considered to investigate the effect of high SSA fractions on CCN concentrations. The first
593 case is an external mixture of 40% nss-sulfate and 60% SSA, representing nominal values for
594 the peak of the high SSA event. The second case was 100% nss-sulfates representing

595 conditions with no sub-100 nm SSA. Using the calculated κ values the critical diameter was
596 calculated as a function of supersaturation. CCN concentrations were calculated by
597 integrating the size distributions above the critical diameter. The CCN activation ratio is the
598 ratio of CCN concentration to condensation nuclei (CN) concentration. CN concentrations
599 were calculated by integrating the entire size distribution. An average size distribution for the
600 period 6:00 to 9:00 8 December 2007 was used for the high SSA mode case and an average
601 over 10:00 to 15:00 7 December for the case with no sub-100 nm SSA. The total integrated
602 concentrations for the high SSA particle case and no SSA particles case were 347 and 368
603 cm^{-3}, respectively. Therefore the enhancements in absolute CCN concentrations shown in
604 Figure 7A were due to the increased proportion of SSA, rather than an increase in overall
605 particle concentrations.

606 The supersaturation at which a population of particles were initially activated into droplets
607 can be estimated by applying the particle diameter at the Hoppel minimum as the critical
608 diameter for droplet formation [*Blot et al.*, 2013]. Estimated supersaturations range from 0.25
609 to 0.38% and 0.13 to 0.2% using the κ calculated from the HGFs for the nss-sulfate and SSA
610 modes, respectively. This provides a guide for the typical cloud supersaturation in the
611 Southern Ocean south of Australia during the study period. Enhancement of the CCN
612 activation ratio is observed with the presence of sea salt (Figure 7). The enhancement in the
613 CCN activation ratio is 8.4% at 0.2% supersaturation and 8.7% at 0.4% supersaturation. It
614 should be noted that the skill of subsaturated H-TDMA measurements to represent CCN
615 concentrations is an ongoing research question. For example *Good et al.* [2010a] identified an
616 increase in the disagreement between measured CCN number concentration and that
617 calculated using H-TDMA methods with supersaturations below 0.2%. Nevertheless an
618 enhancement in CCN with increasing sea salt is to be expected due to its hygroscopic

619 properties. Determination of the influence of the enhancement of CCN concentrations on
620 cloud properties requires further modelling.

621 **5. Conclusions**

622 Large concentrations of sub-100 nm SSA particles ranging in size from 16 to 97 nm diameter
623 were observed at Cape Grim, Tasmania in clean, marine conditions on 7 – 8 December 2007.
624 Two externally mixed modes were observed in the HGF distributions, the SSA mode with
625 very high HGFs and another mode with moderate HGFs. The moderate HGF mode displayed
626 volatility consistent with ammonium sulfate and prompt deliquescence at 79-80% RH,
627 providing strong evidence that this mode is dominated by nss-sulfates. The SSA particles
628 were refractory (up to 280 °C) and they deliquesced promptly at 73-75% RH, which further
629 confirmed their identity as SSA particles with a large proportion of inorganic sea salt. The
630 HGFs at 90% of the ambient SSA particles were suppressed relative to those for pure sea salt,
631 which suggests the inorganic sea salt may have been internally mixed with a non-volatile
632 organic component. Continuous HGF measurements provided a temporal characterisation for
633 the SSA event. Number fractions of the SSA mode peaked at 69%, corresponding to an
634 estimated sub-100 nm SSA concentration of 110-290 cm^{-3}.

635 Measurements of sub-100 nm inorganic SSA are scarce, particularly for the Southern
636 Hemisphere. The observation and characterisation of 16 to 97 nm diameter SSA is a unique
637 set of measurements. Based on the measured HGFs, the organic volume fraction of the SSA
638 was calculated to be 11 – 46%. This result is contrary to summertime primary marine aerosol
639 observations from the North Atlantic and Pacific Oceans [*O'Dowd et al.*, 2004; *Facchini et*
640 *al.*, 2008; *Quinn et al.*, 2014], which show a greater sub-100 nm organic fraction.
641 Additionally, these previous studies observed increased organic enrichment with decreasing
642 particle size. In this study, HGFs increased with decreasing particle size, which indicates the

643 possibility of a reduced organic fraction at smaller sizes. Discrepancies in observed size
644 dependant organic SSA fraction suggest that organic enrichment is not necessarily spatial
645 uniform during periods of high biological activity. Simultaneous TEM and X-ray
646 spectrometry of sub-100 nm mode aerosols collected from the same location, and at the same
647 time, displayed a distinct lack of sea salt and appear to be made up of organic aggregates and
648 microgels [*Leck and Bigg*, 2010]. As strong evidence of the existence of a large sea salt
649 fraction (high HGF, non volatile up to 280°C, deliquescence at 75% RH) has been presented
650 in this study we highlight the potential biases of other techniques in analysis of the chemical
651 composition of marine aerosols. Further inter-comparison studies are needed to properly
652 quantify the composition of sub-100 nm SSA.

653 Analysis of air mass back trajectories indicated that the SSA particles observed at Cape Grim
654 were produced 1500 km upwind in the Southern Ocean during high wind speed events (12-20
655 ms^{-1}). The arrival of SSA particles at the site coincided with moderate increases in 3-10 nm
656 particle concentrations (hourly averages of up to 170 cm^{-3}), which were likely due to the
657 entrainment of air from the free troposphere following the passing of a cold front [*Gras et al.*,
658 2009]. We suggest the dropping boundary layer on the morning of 8 December could have
659 contributed to an enhanced SSA number fraction. Although this event does not provide
660 information on the long-term sub-100 nm particle composition at Cape Grim it provides
661 details on the ambient SSA composition and the factors that control SSA concentrations in
662 the atmosphere.

663 **Acknowledgements**

664 The authors gratefully acknowledge the NOAA Air Resources Laboratory (ARL) for the
665 provision of the HYSPLIT transport and dispersion model used in this publication. CSIRO
666 and the Australian Bureau of Meteorology in Australia are also thanked for their continuous

667 support of Cape Grim BAPS. We also thank Wlodek Zaharowski from ANSTO for supplying
668 radon data and the staff at the Cape Grim Baseline Air Pollution Station in Tasmania. All
669 results presented in this study and associated data are available from the corresponding author
670 on request via email, z.ristovski@qut.edu.au.

671 **References**

672 Allan, J. D. et al. (2009), Composition and properties of atmospheric particles in the eastern
673 Atlantic and impacts on gas phase uptake rates, *Atmos. Chem. Phys.*, *9*(23), 9299–9314,
674 doi:10.5194/acp-9-9299-2009.

675 Andreae, M. O. (1982), Marine aerosol chemistry at Cape Grim, Tasmania, and Townsville,
676 Queensland, *J. Geophys. Res.*, *87*(C11), 8875–8885, doi:10.1029/JC087iC11p08875.

677 Andreae, M. O., and D. Rosenfeld (2008), Aerosol–cloud–precipitation interactions. Part 1.
678 The nature and sources of cloud-active aerosols, *Earth-Science Reviews*, *89*(1), 13–41.

679 Atlas, R., R. N. Hoffman, J. Ardizzone, S. M. Leidner, J. C. Jusem, D. K. Smith, and D.
680 Gombos (2013), A Cross-calibrated, Multiplatform Ocean Surface Wind Velocity
681 Product for Meteorological and Oceanographic Applications, *Bull. Amer. Meteor. Soc.*,
682 *92*(2), 157–174, doi:doi: 10.1175/2010BAMS2946.1.

683 Ault, A. P. et al. (2013), Size-Dependent Changes in Sea Spray Aerosol Composition and
684 Properties with Different Seawater Conditions, *Environ. Sci. Technol.*, *47*(11), 5603–
685 5612, doi:doi: 10.1021/es400416g.

686 Baines, P. G., and D. Murray (1994), Modelling of the airflow over Cape Grim, *Baseline*
687 *Atmospheric Program (Australia) 1991*, 20–24.

688 Bates, T. S. et al. (2012), Measurements of ocean derived aerosol off the coast of California,
689 *J. Geophys. Res.*, *117*(D12), n/a–n/a, doi:10.1029/2012JD017588.

690 Bates, T. S., V. N. Kapustin, P. K. Quinn, D. S. Covert, D. J. Coffman, C. Mari, P. A.
691 Durkee, W. J. De Bruyn, and E. S. Saltzman (1998), Processes controlling the
692 distribution of aerosol particles in the lower marine boundary layer during the First
693 Aerosol Characterization Experiment (ACE 1), *J. Geophys. Res.*, *103*(D13), 16369–
694 16383, doi:10.1029/97JD03720.

695 Berg, O. H., E. Swietlicki, and R. Krejci (1998), Hygroscopic growth of aerosol particles in
696 the marine boundary layer over the Pacific and Southern Oceans during the First Aerosol
697 Characterization Experiment (ACE 1), *J. Geophys. Res.*, *103*(D13), 16535–16545.

698 Bialek, J., M. Dall'Osto, C. Monahan, D. Beddows, and C. O'Dowd (2012), On the
699 contribution of organics to the North East Atlantic aerosol number concentration,
700 *Environ. Res. Lett.*, *7*(4), 044013, doi:10.1088/1748-9326/7/4/044013.

701 Bigg, E. K. (2007), Sources, nature and influence on climate of marine airborne particles,

Environ. Chem., *4*(3), 155–161, doi:10.1071/EN07001.

Bigg, E. K., and C. Leck (2008), The composition of fragments of bubbles bursting at the ocean surface, *J. Geophys. Res.*, *113*(D11), D11209, doi:10.1029/2007JD009078.

Biskos, G., A. Malinowski, L. M. Russell, P. R. Buseck, and S. T. Martin (2006a), Nanosize Effect on the Deliquescence and the Efflorescence of Sodium Chloride Particles, *Aerosol Science and Technology*, *40*(2), 97–106, doi:10.1080/02786820500484396.

Biskos, G., D. Paulsen, L. M. Russell, P. R. Buseck, and S. T. Martin (2006b), Prompt deliquescence and efflorescence of aerosol nanoparticles, *Atmos. Chem. Phys.*, *6*(12), 4633–4642.

Biskos, G., L. M. Russell, P. R. Buseck, and S. T. Martin (2006c), Nanosize effect on the hygroscopic growth factor of aerosol particles, *Geophys. Res. Lett.*, *33*(7), n/a–n/a, doi:10.1029/2005GL025199.

Blot, R., A. D. Clarke, S. Freitag, V. Kapustin, S. G. Howell, J. B. Jensen, L. M. Shank, C. S. McNaughton, and V. Brekhovskikh (2013), Ultrafine sea spray aerosol over the southeastern Pacific: open-ocean contributions to marine boundary layer CCN, *Atmos. Chem. Phys.*, *13*(14), 7263–7278, doi:10.5194/acp-13-7263-2013.

Burrows, S. M., O. Ogunro, A. A. Frossard, L. M. Russell, P. J. Rasch, and S. Elliott (2014), A physically-based framework for modelling the organic fractionation of sea spray aerosol from bubble film Langmuir equilibria, *Atmospheric Chemistry and Physics Discussions*, *14*(5), 5375–5443, doi:10.5194/acpd-14-5375-2014.

Carslaw, K. S. et al. (2013), Large contribution of natural aerosols to uncertainty in indirect forcing, *Nature*, *503*(7474), 67–71, doi:Article.

Ceburnis, D., C. D. O'Dowd, G. S. Jennings, M. C. Facchini, L. Emblico, S. Decesari, S. Fuzzi, and J. Sakalys (2008), Marine aerosol chemistry gradients: Elucidating primary and secondary processes and fluxes, *Geophys. Res. Lett.*, *35*(7), n/a–n/a, doi:10.1029/2008GL033462.

Chen, H., J. Sangster, T. T. Teng, and F. Lenzi (1973), A general method of predicting the water activity of ternary aqueous solutions from binary data, *Can. J. Chem. Eng.*, *51*(2), 234–241, doi:10.1002/cjce.5450510214.

Collins, D. B. et al. (2013), Impact of marine biogeochemistry on the chemical mixing state and cloud forming ability of nascent sea spray aerosol, *J. Geophys. Res. Atmos.*, n/a–n/a, doi:10.1002/jgrd.50598.

de Leeuw, G., E. L. Andreas, M. D. Anguelova, C. W. Fairall, E. R. Lewis, C. O'Dowd, M. Schulz, and S. E. Schwartz (2011), Production flux of sea spray aerosol, *Rev. Geophys.*, *49*(2), n/a–n/a, doi:10.1029/2010RG000349.

Draxler, R. R., and G. D. Rolph (Eds.) (2013), *HYSPLIT(HYbrid Single-PArticle Lagrangian Intergrated Trajectory) Model*, NOAA Air Resources Laboratory, College Park, MD. Available from: http://www.arl.noaa.gov/HYSPLIT.php (Accessed 1 September 2013)

Facchini, M. C. et al. (2008), Primary submicron marine aerosol dominated by insoluble

741 organic colloids and aggregates, *Geophys. Res. Lett.*, *35*(17), n/a–n/a.

742 Fletcher, C. A., G. R. Johnson, Z. D. Ristovski, and M. Harvey (2007), Hygroscopic and
743 volatile properties of marine aerosol observed at Cape Grim during the P2P campaign,
744 *Environ. Chem.*, *4*(3), 162–171, doi:10.1071/EN07011.

745 Fuentes, E., H. Coe, D. Green, and G. McFiggans (2011), On the impacts of phytoplankton-
746 derived organic matter on the properties of the primary marine aerosol – Part 2:
747 Composition, hygroscopicity and cloud condensation activity, *Atmos. Chem. Phys.*,
748 *11*(6), 2585–2602, doi:10.5194/acp-11-2585-2011.

749 Fuentes, E., H. Coe, D. Green, G. de Leeuw, and G. McFiggans (2010), Laboratory-generated
750 primary marine aerosol via bubble-bursting and atomization, *Atmos. Meas. Tech.*, *3*(1),
751 141–162, doi:10.5194/amt-3-141-2010.

752 Gantt, B., and N. Meskhidze (2013), The physical and chemical characteristics of marine
753 primary organic aerosol: a review, *Atmos. Chem. Phys.*, *13*(8), 3979–3996,
754 doi:10.5194/acpd-12-21779-2012.

755 Good, N., D. O. Topping, J. D. Allan, M. Flynn, E. Fuentes, M. Irwin, P. I. Williams, H. Coe,
756 and G. McFiggans (2010a), Consistency between parameterisations of aerosol
757 hygroscopicity and CCN activity during the RHaMBLe discovery cruise, *Atmos. Chem.*
758 *Phys.*, *10*(7), 3189–3203.

759 Good, N., H. Coe, and G. McFiggans (2010b), Instrumentational operation and analytical
760 methodology for the reconciliation of aerosol water uptake under sub- and supersaturated
761 conditions, *Atmos. Meas. Tech.*, *3*(5), 1241–1254, doi:10.5194/amt-3-1241-2010.

762 Gras, J. L. (2009), Postfrontal nanoparticles at Cape Grim: impact on cloud nuclei
763 concentrations, *Environ. Chem.*, *6*(6), 515–523, doi:10.1071/EN09076.

764 Gras, J. L. (2011), Particles, in *Baseline Atmospheric Program, Australia*, edited by N. Derek
765 and P. B. Krummel, CSIRO and BoM.

766 Gras, J. L., and G. P. Ayers (1983), Marine aerosol at southern mid-latitudes, *J. Geophys.*
767 *Res.*, *88*(C15), 10661–10666, doi:10.1029/JC088iC15p10661.

768 Gras, J. L., S. I. Jimi, S. T. Siems, and P. B. Krummel (2009), Postfrontal nanoparticles at
769 Cape Grim: observations, *Environ. Chem.*, *6*(6), 508–514, doi:10.1071/EN09075.

770 Gysel, M., E. Weingartner, S. Nyeki, D. Paulsen, U. BALTENSPERGER, I. Galambos, and
771 G. Kiss (2004), Hygroscopic properties of water-soluble matter and humic-like organics
772 in atmospheric fine aerosol, *Atmos. Chem. Phys.*, *4*(1), 35–50, doi:10.5194/acp-4-35-
773 2004.

774 Gysel, M., G. B. McFiggans, and H. Coe (2009), Inversion of tandem differential mobility
775 analyser (TDMA) measurements, *Journal of Aerosol Science*, *40*(2), 134–151,
776 doi:10.1016/j.jaerosci.2008.07.013.

777 Heintzenberg, J., W. Birmili, A. Wiedensohler, A. Nowak, and T. Tuch (2011), Structure,
778 variability and persistence of the submicrometre marine aerosol, *Tellus B*, *56*(4).

779 Hoppel, W. A., G. M. Frick, and R. E. Larson (1986), Effect of nonprecipitating clouds on
780 the aerosol size distribution in the marine boundary layer, *Geophys. Res. Lett.*, *13*(2),
781 125–128, doi:10.1029/GL013i002p00125.

782 Johnson, G. R., C. Fletcher, N. Meyer, R. Modini, and Z. D. Ristovski (2008), A robust,
783 portable H-TDMA for field use, *Journal of Aerosol Science*, *39*(10), 850–861,
784 doi:10.1016/j.jaerosci.2008.05.005.

785 Johnson, G. R., Z. Ristovski, and L. Morawska (2004), Method for measuring the
786 hygroscopic behaviour of lower volatility fractions in an internally mixed aerosol,
787 *Journal of Aerosol Science*, *35*(4), 443–455, doi:10.1016/j.jaerosci.2003.10.008.

788 Jones, A., D. Thomson, M. Hort, and B. Devenish (2007), The U.K. Met Office's Next-
789 Generation Atmospheric Dispersion Model, NAME III, in *Air Pollution Modeling and Its*
790 *Application XVII*, edited by C. Borrego and A.-L. Norman, pp. 580–589, Springer US.

791 Kanamitsu, M. (1989), Description of the NMC Global Data Assimilation and Forecast
792 System, *Wea. Forecasting*, *4*(3), 335–342, doi:10.1175/1520-
793 0434(1989)004<0335:DOTNGD>2.0.CO;2.

794 Keene, W. C. et al. (2007), Chemical and physical characteristics of nascent aerosols
795 produced by bursting bubbles at a model air-sea interface, *J. Geophys. Res.*, *112*(D21),
796 n/a–n/a.

797 Kreidenweis, S. M., L. M. Mclnnes, and F. J. Brechtel (1998), Observations of aerosol
798 volatility and elemental composition at Macquarie Island during the First Aerosol
799 Characterization Experiment (ACE 1), *J. Geophys. Res.*, *103*(D13), 16511–16–524.

800 Laskin, A., R. C. Moffet, M. K. Gilles, J. D. Fast, R. A. Zaveri, B. Wang, P. Nigge, and J.
801 Shutthanandan (2012), Tropospheric chemistry of internally mixed sea salt and organic
802 particles: Surprising reactivity of NaCl with weak organic acids, *J. Geophys. Res.*,
803 *117*(D15), D15302, doi:10.1029/2012JD017743.

804 Leck, C., and E. K. Bigg (2010), New particle formation of marine biological origin, *Aerosol*
805 *Science and Technology*, *44*(7), 570–577.

806 Leck, C., and E. K. Bigg (2005a), Biogenic particles in the surface microlayer and overlaying
807 atmosphere in the central Arctic Ocean during summer, *Tellus B*, *57*(4), 305–316,
808 doi:10.1111/j.1600-0889.2005.00148.x.

809 Leck, C., and E. K. Bigg (2005b), Source and evolution of the marine aerosol—A new
810 perspective, *Geophys. Res. Lett.*, *32*(19), n/a–n/a.

811 Leck, C., and E. K. Bigg (2008), Comparison of sources and nature of the tropical aerosol
812 with the summer high Arctic aerosol, *Tellus B*, *60*(1), 118–126, doi:10.1111/j.1600-
813 0889.2007.00315.x.

814 Lewis, E. R., and S. E. Schwartz (2004), *Sea salt aerosol production: mechanisms, methods,*
815 *measurements and models: a critical review*, Amer Geophysical Union.

816 Mårtensson, E. M., E. D. Nilsson, G. de Leeuw, L. H. Cohen, and H. C. Hansson (2003),
817 Laboratory simulations and parameterization of the primary marine aerosol production, *J.*

818 *Geophys. Res.*, *108*(D9), n/a–n/a, doi:10.1029/2002JD002263.

819 Mertes, S., F. Schröder, and A. Wiedensohler (1995), The Particle Detection Efficiency
820 Curve of the TSI-3010 CPC as a Function of the Temperature Difference between
821 Saturator and Condenser, *Aerosol Science and Technology*, *23*(2), 257–261,
822 doi:10.1080/02786829508965310.

823 Middlebrook, A. M., D. M. Murphy, and D. S. Thomson (1998), Observations of organic
824 material in individual marine particles at Cape Grim during the First Aerosol
825 Characterization Experiment (ACE 1), *J. Geophys. Res.*, *103*(D13), 16475–16483,
826 doi:10.1029/97JD03719.

827 Mikhailov, E., S. Vlasenko, R. Niessner, and U. P oschl (2004), Interaction of aerosol
828 particles composed of protein and saltswith water vapor: hygroscopic growth and
829 microstructural rearrangement, *Atmos. Chem. Phys.*, *4*(2), 323–350, doi:10.5194/acp-4-
830 323-2004.

831 Modini, R. L., B. Harris, and Z. Ristovski (2010a), The organic fraction of bubble-generated,
832 accumulation mode Sea Spray Aerosol (SSA), *Atmos. Chem. Phys.*, *10*(6), 2867–2877.

833 Murphy, D. M., D. S. Thomson, A. M. Middlebrook, and M. E. Schein (1998a), In situ
834 single-particle characterization at Cape Grim, *J. Geophys. Res.*, *103*(D13), 16485–16491,
835 doi:10.1029/97JD03281.

836 Murphy, D. M., D. S. Thomson, and A. M. Middlebrook (1997), Bromine, iodine, and
837 chlorine in single aerosol particles at Cape Grim, *Geophys. Res. Lett.*, *24*(24), 3197–
838 3200, doi:10.1029/97GL03195.

839 Murphy, D. M., J. R. Anderson, P. K. Quinn, L. M. McInnes, F. J. Brechtel, S. M.
840 Kreidenweis, A. M. Middlebrook, M. Posfai, D. S. Thomson, and P. R. Buseck (1998b),
841 Influence of sea-salt on aerosol radiative properties in the Southern Ocean marine
842 boundary layer, *Nature*, *392*(6671), 62–65.

843 Niedermeier, D., H. Wex, J. Voigtl ander, F. Stratmann, E. Br uggemann, A. Kiselev, H.
844 Henk, and J. Heintzenberg (2008), LACIS-measurements and parameterization of sea-
845 salt particle hygroscopic growth and activation, *Atmos. Chem. Phys.*, *8*(3), 579–590,
846 doi:10.5194/acp-8-579-2008.

847 O'Dowd, C. D., M. C. Facchini, F. Cavalli, D. Ceburnis, M. Mircea, S. Decesari, S. Fuzzi, Y.
848 J. Yoon, and J.-P. Putaud (2004), Biogenically driven organic contribution to marine
849 aerosol, *Nature*, *431*(7009), 676–680, doi:10.1038/nature02959.

850 Oppo, C., S. Bellandi, N. Degli Innocenti, A. M. Stortini, G. Loglio, E. Schiavuta, and R.
851 Cini (1999), Surfactant components of marine organic matter as agents for
852 biogeochemical fractionation and pollutant transport via marine aerosols, *Marine*
853 *Chemistry*, *63*(3–4), 235–253.

854 Ovadnevaite, J., A. Manders, G. de Leeuw, D. Ceburnis, C. Monahan, A. I. Partanen, H.
855 Korhonen, and C. D. O'Dowd (2014), A sea spray aerosol flux parameterization
856 encapsulating wave state, *Atmos. Chem. Phys.*, *14*(4), 1837–1852, doi:10.5194/acp-14-
857 1837-2014.

858 Ovadnevaite, J., D. Ceburnis, G. Martucci, J. Bialek, C. Monahan, M. Rinaldi, M. C.
859 Facchini, H. Berresheim, D. R. Worsnop, and C. O'Dowd (2011), Primary marine
860 organic aerosol: A dichotomy of low hygroscopicity and high CCN activity, *Geophys.*
861 *Res. Lett.*, *38*(21), L21806, doi:10.1029/2011GL048869.

862 Peng, C., M. N. Chan, and C. K. Chan (2001), The Hygroscopic Properties of Dicarboxylic
863 and Multifunctional Acids: Measurements and UNIFAC Predictions, *Environ. Sci.*
864 *Technol.*, *35*(22), 4495–4501, doi:10.1021/es0107531.

865 Petters, M. D., and S. M. Kreidenweis (2007), A single parameter representation of
866 hygroscopic growth and cloud condensation nucleus activity, *Atmos. Chem. Phys.*, *7*(8),
867 1961–1971.

868 Pósfai, M., J. Li, J. R. Anderson, and P. R. Buseck (2003), Aerosol bacteria over the Southern
869 Ocean during ACE-1, *Atmospheric Research*, *66*(4), 231–240.

870 Prather, K. A. et al. (2013), Bringing the ocean into the laboratory to probe the chemical
871 complexity of sea spray aerosol, *Proceedings of the National Academy of Sciences*,
872 *110*(19), 7550–7555.

873 Quinn, P. K. et al. (2000), Surface submicron aerosol chemical composition: What fraction is
874 not sulfate? *J. Geophys. Res.*, *105*(D5), 6785–6805, doi:10.1029/1999JD901034.

875 Quinn, P. K., T. S. Bates, K. S. Schulz, D. J. Coffman, A. A. Frossard, L. M. Russell, W. C.
876 Keene, and D. J. Kieber (2014), Contribution of sea surface carbon pool to organic matter
877 enrichment in sea spray aerosol, *Nature Geosci*, *7*(3), 228–232, doi:10.1038/ngeo2092.

878 Rinaldi, M. et al. (2009), On the representativeness of coastal aerosol studies to open ocean
879 studies: Mace Head – a case study, *Atmos. Chem. Phys.*, *9*(24), 9635–9646,
880 doi:10.5194/acp-9-9635-2009.

881 Rinaldi, M., S. Decesari, E. Finessi, L. Giulianelli, C. Carbone, S. Fuzzi, C. D. O'Dowd, D.
882 Ceburnis, and M. C. Facchini (2010), Primary and Secondary Organic Marine Aerosol
883 and Oceanic Biological Activity: Recent Results and New Perspectives for Future
884 Studies, *Advances in Meteorology*, *2010*, doi:10.1155/2010/310682.

885 Sellegri, K., J. Gourdeau, J.-P. Putaud, and S. Despiau (2001), Chemical composition of
886 marine aerosol in a Mediterranean coastal zone during the FETCH experiment, *J.*
887 *Geophys. Res.*, *106*(D11), 12023–12037, doi:10.1029/2000JD900629.

888 Stokes, R. H., and R. A. Robinson (1966), Interactions in Aqueous Nonelectrolyte Solutions.
889 I. Solute-Solvent Equilibria, *J. Phys. Chem.*, *70*(7), 2126–2131,
890 doi:10.1021/j100879a010.

891 Swietlicki, E. et al. (2008), Hygroscopic properties of submicrometer atmospheric aerosol
892 particles measured with H-TDMA instruments in various environments - A review,
893 *Tellus, Series B: Chemical and Physical Meteorology*, *60 B*(3), 432–469.

894 Swietlicki, E., J. Zhou, D. S. Covert, K. Hämeri, B. Busch, M. Väkevä, U. Dusek, O. H.
895 Berg, A. Wiedensohler, and P. Aalto (2000), Hygroscopic properties of aerosol particles
896 in the north-eastern Atlantic during ACE-2, *Tellus B*, *52*(2), 201–227.

Tang, I. N., and H. R. Munkelwitz (1994), Water activities, densities, and refractive indices of aqueous sulfates and sodium nitrate droplets of atmospheric importance, *J. Geophys. Res.*, *99*(D9), 18801–18808, doi:10.1029/94JD01345.

Twohy, C. H. et al. (2013), Impacts of aerosol particles on the microphysical and radiative properties of stratocumulus clouds over the southeast Pacific Ocean, *Atmos. Chem. Phys.*, *13*(5), 2541–2562, doi:10.5194/acp-13-2541-2013.

Väkevä, M., K. Hämeri, and P. P. Aalto (2002), Hygroscopic properties of nucleation mode and Aitken mode particles during nucleation bursts and in background air on the west coast of Ireland, *J. Geophys. Res.*, *107*(D19), PAR 9–1–PAR 9–11, doi:10.1029/2000JD000176.

Wise, M. E., E. J. Freney, C. A. Tyree, J. O. Allen, S. T. Martin, L. M. Russell, and P. R. Buseck (2009), Hygroscopic behavior and liquid-layer composition of aerosol particles generated from natural and artificial seawater, *J. Geophys. Res.*, *114*(D3), D03201, doi:10.1029/2008JD010449.

Zahorowski, W., S. D. Chambers, and A. Henderson-Sellers (2004), Ground based radon-222 observations and their application to atmospheric studies, *Journal of Environmental Radioactivity*, *76*(1–2), 3–33.

Zahorowski, W., S. D. Chambers, and J. Crawford (2011), Radon and radon daughters, in *Baseline atmospheric program, Australia.*, edited by N. Derek and P. B. Krummel, CSIRO and BoM.

Zhou, J., E. Swietlicki, O. H. Berg, P. P. Aalto, K. Hämeri, E. D. NILSSON, and C. Leck (2001), Hygroscopic properties of aerosol particles over the central Arctic Ocean during summer, *J. Geophys. Res.*, *106*(D23), 32111–32123.

923 Table 1: Organic fraction observed from nascent SSA measurements.

Source	Location	Season	Measurement technique (s) [1]	Particle size	Organic Fraction [2]	Weighting factor
Quinn et al. 2014	North West Atlantic	Autumn	CCNc	100nm ; 40 nm	40%; 80%	volume
Facchini et al. 2008	North East Atlantic	Summer	IC, TOC, EGA, HNMR	125-250nm	77%	mass
Prather et al. 2013; Collins et al. 2013	North East Pacific	Autumn	TEM-EDX, AMS, CCNc, DASH-SP	60-180 nm	OC 26% SS-OC 55%	number
Keene et al. 2007	North West Atlantic	Autumn	IC, TOC	130 nm	80%	mass
Modini et al. 2010	South west Pacific	Summer	VH-TDMA	71-77 nm	8%	volume
					4%	mass
Fuentes et al. 2011	Model equatorial Atlantic seawater	-	H-TDMA, CCNc	40-240 nm	8-37%	volume

924 1. CCNc (cloud condensation nuclei counter), IC (ion chromatography), TOC (total organic carbon), EGA
925 (evolved gas analysis), HNMR (proton nuclear magnetic resonance), TEM-EDX (transmission electron
926 microscopy with energy dispersive x-ray), AMS (aerosol mass spectrometry), DASH-SP().

927 2. All assumed to be internally mixed with sea salt except for [*Prather et al.*, 2013], which indicates an external
928 mixture of organics (OC) and sea salt internally mixed with organics (SS-OC).

929

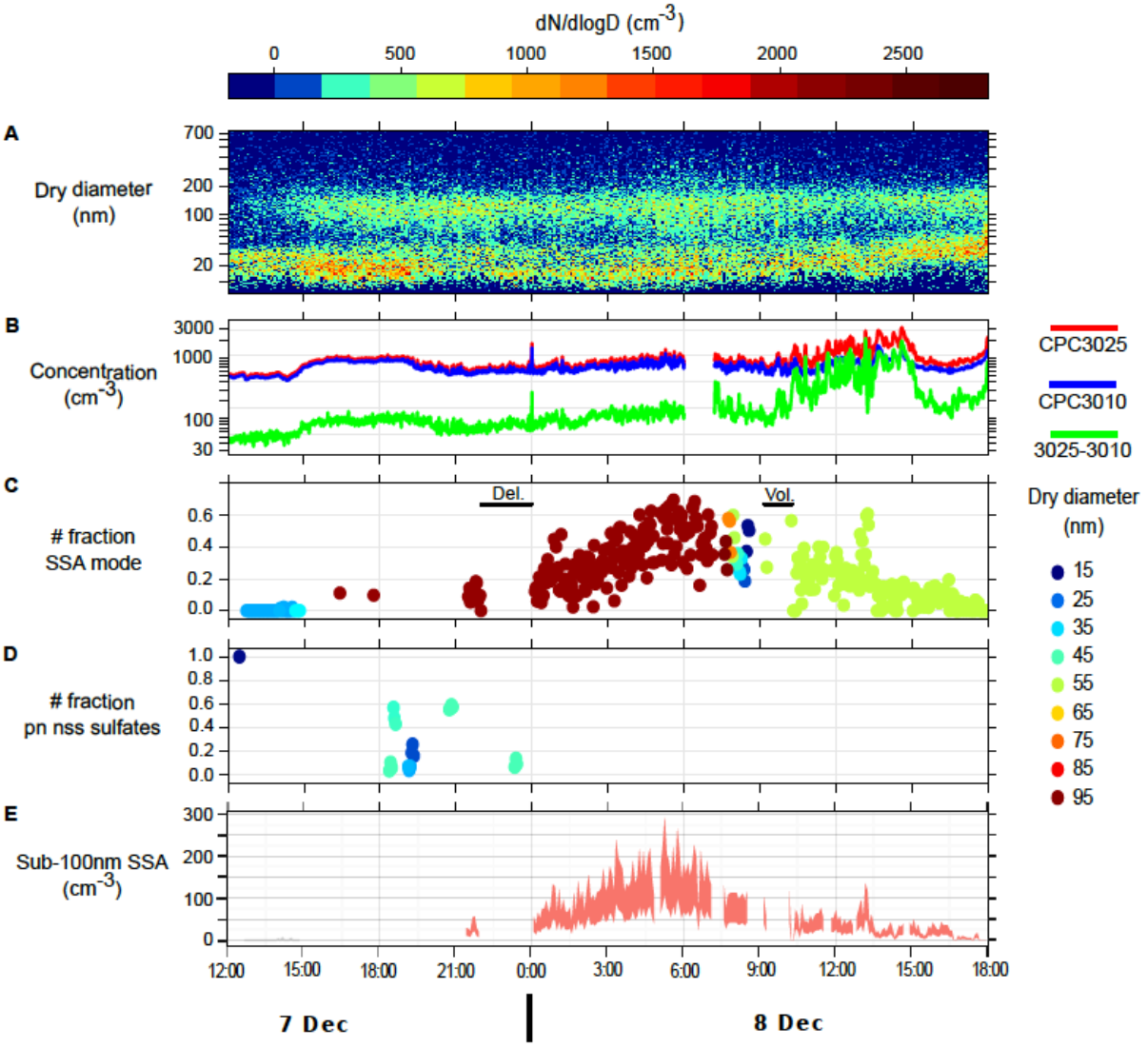

930

931 Figure 1: Time series of particle size distributions (A), particle number concentration (B),
932 number fraction of SSA mode particles (C), number fraction of partially neutralised (pn) nss-
933 sulfates (D) and the concentration of sub-100 nm SSA (E) from 12:00 7/12/07 to 18:00
934 8/12/07. Particle number concentrations measured using TSI3010 CPC (blue), TSI3025 (red)
935 and the difference between TSI3025 and TSI3010 (green). SSA mode defined by HGF>1.85
936 at 90% RH. Horizontal bars in C show periods when particle deliquescence (Del.) and
937 volatility (Vol.) were being measured. Partially neutralised (pn) nss-sulfate measured as
938 number fraction of more hygroscopic mode at 74-76% RH. Sub-100 nm SSA estimated from
939 size dependant very high HGF fraction and size distribution.

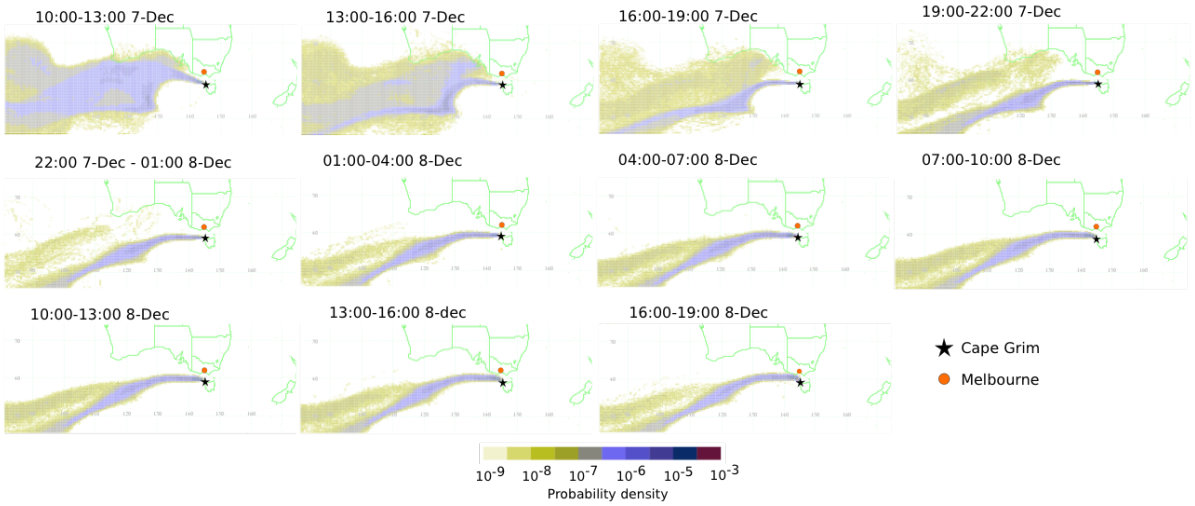

940

941 Figure 2: Air origin probability density maps for the Cape Grim monitoring station, 4am
942 8/12/2007 to 1 pm 8/12/2007 [*Jones et al.*, 2007].

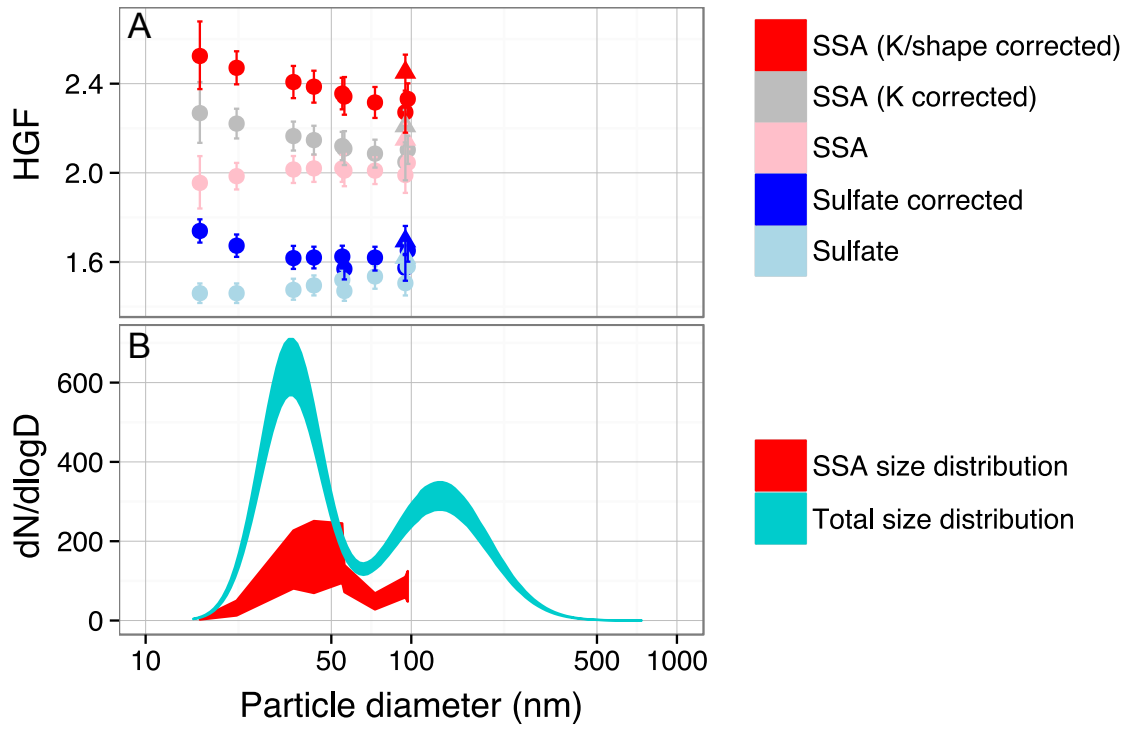

943

944 Figure 3: HGF at 90% RH for the SSA (red, pink and grey) and nss-sulfate (blue and light
945 blue) particles at mobility diameters from 16 to 97 nm (A). Dark markers are Kelvin and
946 shape factor corrected, light markers are raw HGFs and grey markers are Kelvin (not shape)
947 corrected SSA. Kelvin and shape corrected growth factors for 95 nm particles observed

948 overnight are represented by triangles. Size distributions for average total (green) and sub-
949 100 nm SSA (red) particles (B). All observations taken between 07:30 and 08:40 8
950 December. Range in size distributions represents variation in concentration and SSA fraction
951 between 07:30 and 08:40.

952

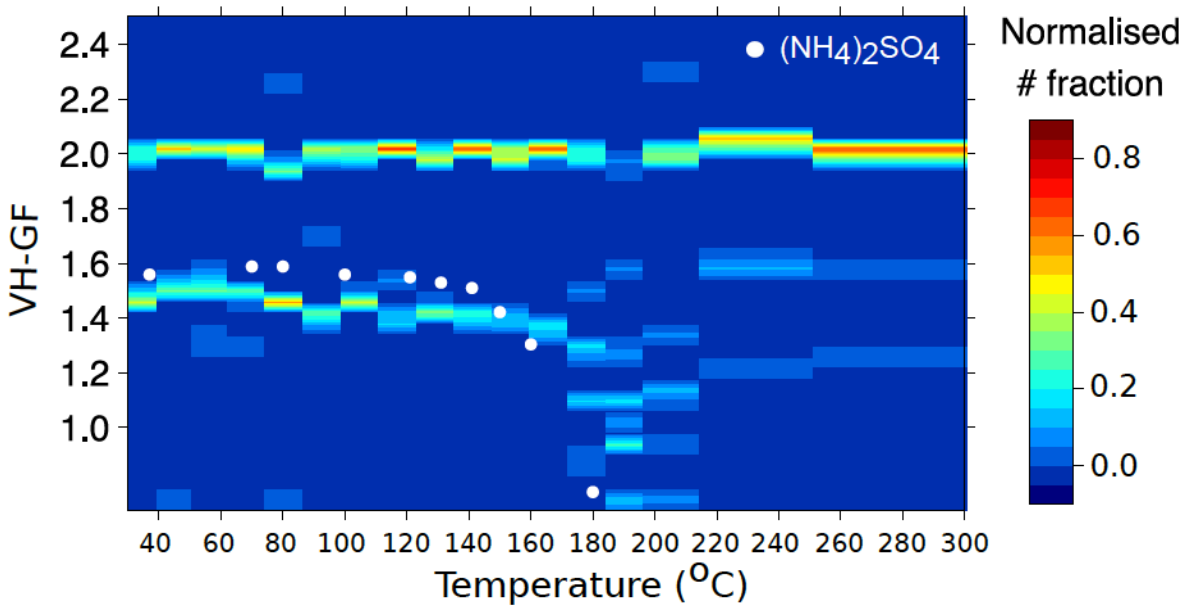

953

954 Figure 4: Volatility of 56 nm ambient marine aerosol observed during high SSA mode event
955 on 8 December 2007 at Cape Grim. Temperature scan undertaken between 09:10 and 10:15 8
956 December 2007. Normalised number fraction indicated by colour scale. Growth factor is ratio
957 of heated, humidified (90% RH) particle diameter to initial particle diameter, 56 nm.
958 Volatility of laboratory generated $(NH_4)_2SO_4$ particles displayed for reference.

959

960

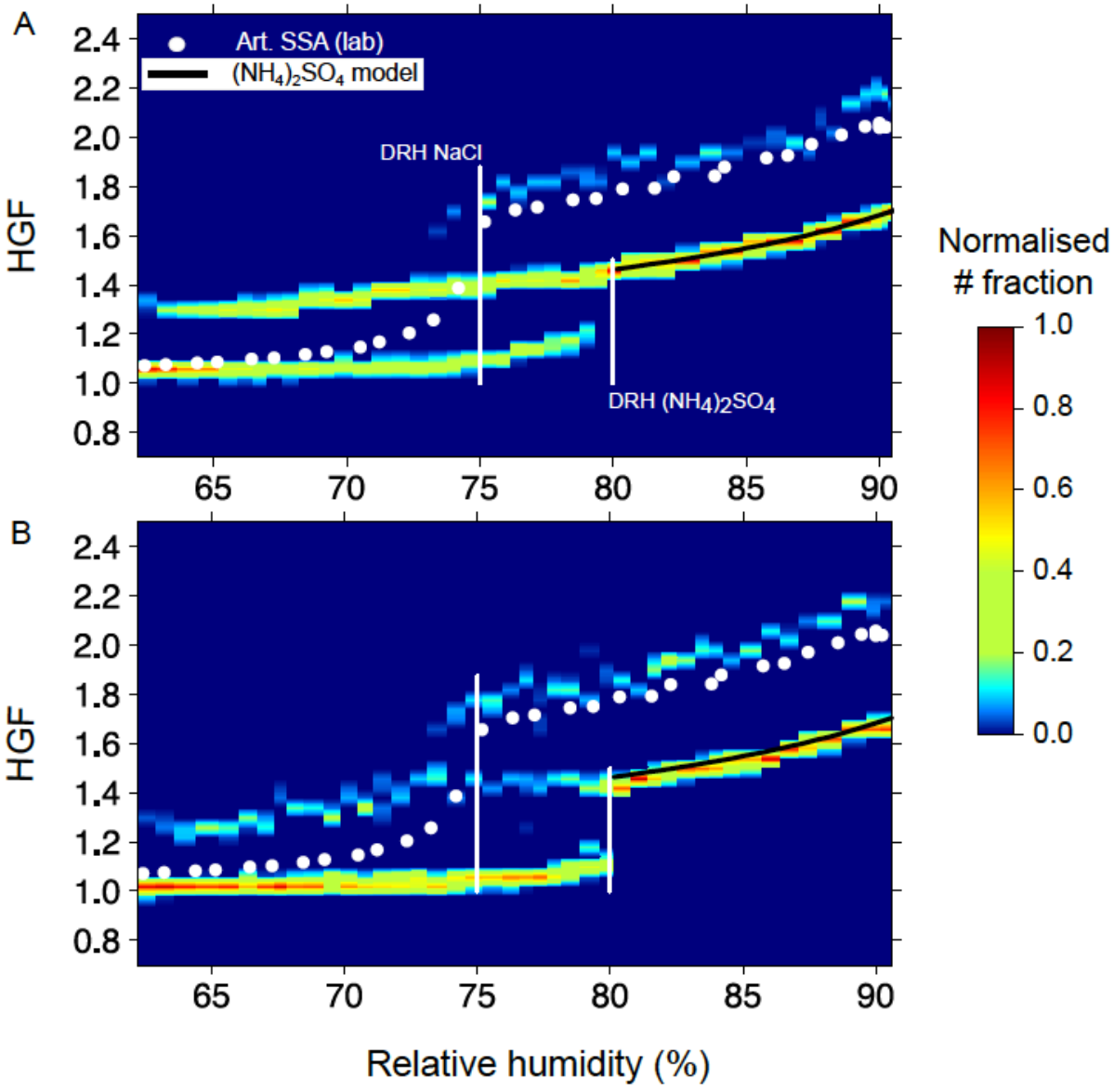

961

962 Figure 5: Deliquescence of 95nm ambient marine aerosol particles at Cape Grim, 22:00-
963 23:00 (A) and 23:00-23:59 (B) 7 December 2007. Normalised number fraction indicated by
964 colour scale. Modelled $(NH_4)_2SO_4$ and laboratory measured artificial SSA (not shape
965 corrected) are indicated by white circles and black lines, respectively [*Fletcher et al.*, 2007].
966 Deliquescence relative humidity (DRH) for NaCl [*Biskos et al.*, 2006a] and $(NH_4)_2SO_4$
967 [*Fletcher et al.*, 2007; *Johnson et al.*, 2008] indicated with white lines.

968

969 Table 2: Selected sub-100 nm primary marine aerosol observations. SSA fractions are
970 maximum fractions indicated in study. SSA fraction in TDMA studies identified by HGF,
971 and therefore generally contain a large fraction of inorganic sea salt.

Source	Particle Diameter (nm)	Location	Season	Method	Sea spray fraction[a]
Bialek et al. [2012]	35-165	Mace Head/ North Atlantic	All	H-TDMA	11-40%
O'Dowd et al. [2004]	60-125	Mace Head/ North Atlantic	Spring/Summer	Filter samples, Ion chromatography	64% [b]
Mårtensson et al. [2003]	35	Tenerife/ West Atlantic	Summer	H-TDMA	11%
	50	Tenerife/ West Atlantic	Summer	H-TDMA	12%
	73	Tenerife/ West Atlantic	Summer	H-TDMA	14%
Fletcher et al. [2007]	100	Cape Grim (Southern Ocean)	Summer	VH-TDMA	15%
Berg et al. [1998]	35	Pacific Ocean	Spring	H-TDMA	15%
	50	Pacific Ocean	Spring	H-TDMA	13%
	75	Pacific Ocean	Spring	H-TDMA	12%
	50	Southern Ocean	Spring/summer	H-TDMA	23%
Zhou et al. [2001]	35	Arctic Ocean	Summer	H-TDMA	100%
	50	Arctic Ocean	Summer	H-TDMA	95%
This study	16-97	Cape Grim	Summer	VH-TDMA	69%

972 [a] Number fraction unless otherwise stated. SSA fraction identified as SSA due to the presence
973 of a sea salt component (from HGF, see Section 2.3), unless otherwise stated.

974 [b] Mass fraction, SSA assumed to be comprised of sea salt and water insoluble organic matter
975 [*O'Dowd et al.*, 2004; *Ceburnis et al.*, 2008; *Facchini et al.*, 2008], dominated by organics
976 (<10% sea salt).

977

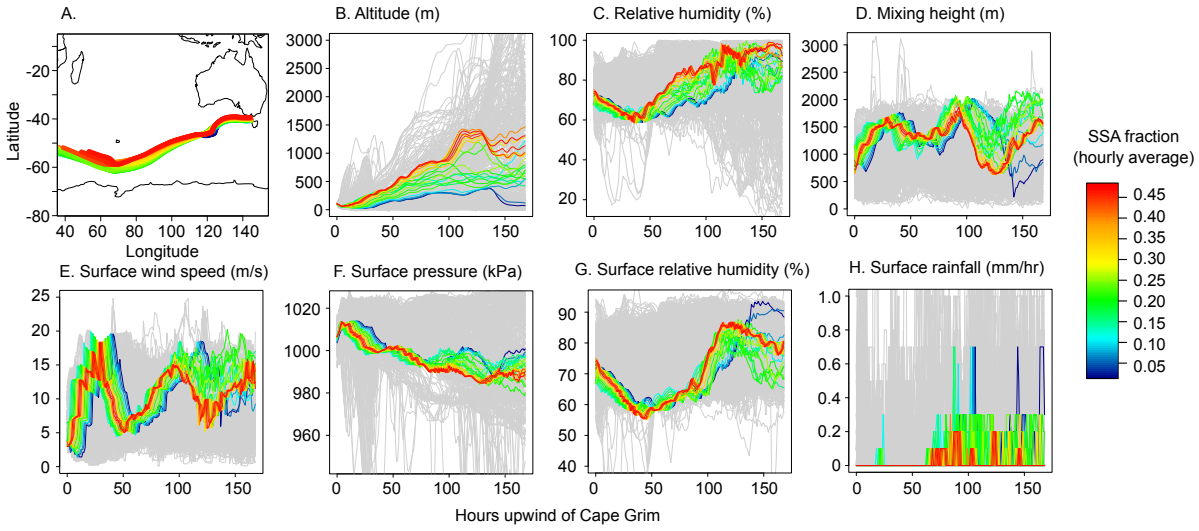

978

979 Figure 6: Hourly back trajectories (7 day) for the high SSA mode event 7-8 Dec. Back
980 trajectory map (A), altitude (B), relative humidity (C) and mixing ratio (D) shown on top, left
981 to right. Surface wind speed (E), pressure (F), relative humidity (G) and rainfall (H) shown
982 on bottom left to right. Back trajectories during the high SSA event are coloured by hourly
983 averaged SSA fraction measured at Cape Grim and all other trajectories during the
984 measurement campaign are shown in grey.

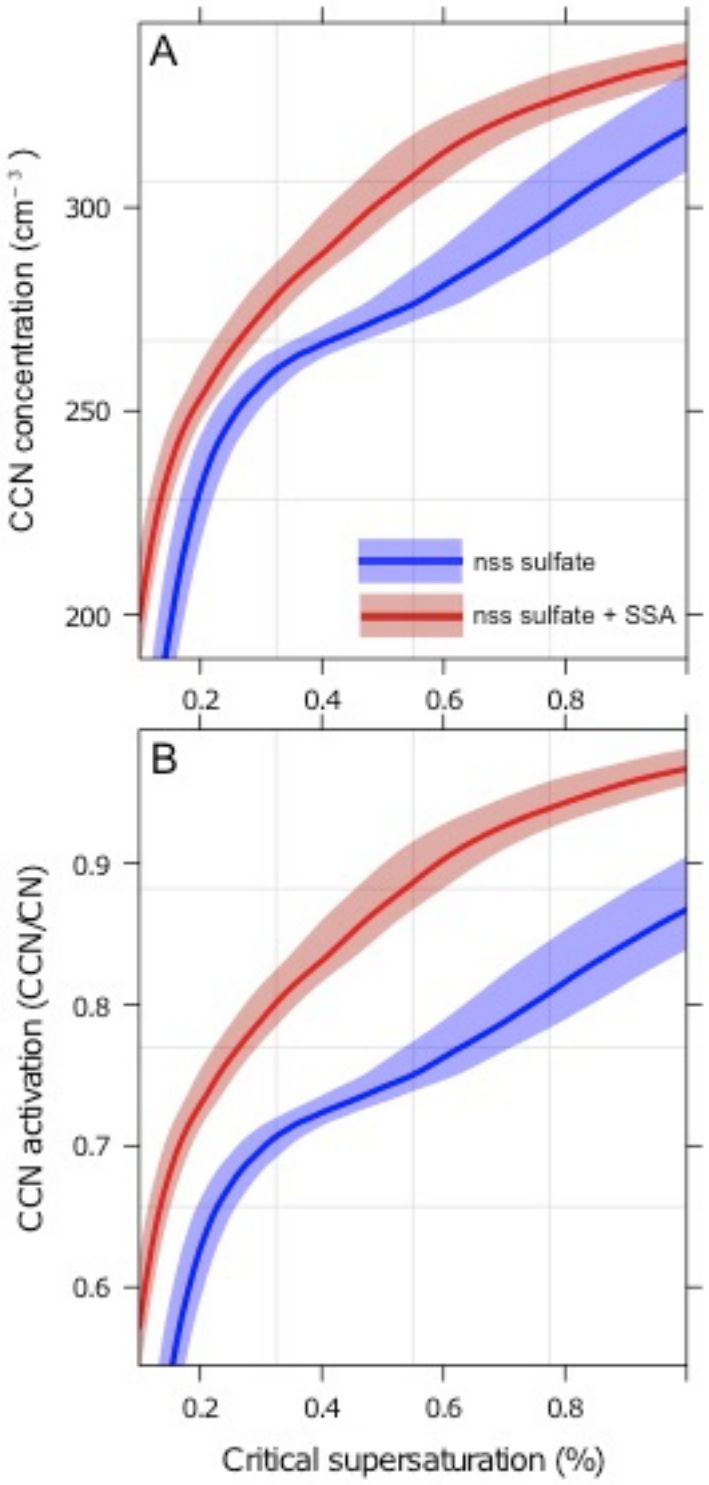

985

986 Figure 7: CCN concentrations (A) and activated fraction, ratio of CCN conc. to CN conc. (B).
987 60% SSA aerosol/40% sulfate (red line) is bounded (red shading) by the CCN activated
988 fraction calculated using minimum and maximum κ from HGF measurements at all measured
989 sizes (including uncertainty). 100% sulfate aerosol (blue line) is bounded (blue shading) by

the CCN activated fraction calculated using minimum and maximum κ from HGF measurements at all sizes (including uncertainty). All calculations for 25°C.